A precision desktop plate-to-roll apparatus for development of advanced flexographic printing processes

Dhanushkodi Mariappan[1], Sanha Kim[1,2], and A. John Hart[1]*

[1]Department of Mechanical Engineering, Massachusetts Institute of Technology, Cambridge, MA 02139, USA.

[2]Department of Mechanical Engineering, Korea Advanced Institute of Science and Technology, Daejeon 34141, South Korea.

*Corresponding author: ajhart@mit.edu

Highlights

- A desktop plate-to-roll printing apparatus for flexographic printing
- Printing with nanoporous stamps by precise stamp-substrate contact force application and elimination of shear; Flexure based contact force application and coordinated rotary-linear motion
- High-speed (>0.1 m/s) printing of high-resolution (<3 microns) features

A precision desktop plate-to-roll apparatus for development of advanced flexographic printing processes

Dhanushkodi Mariappan[1], Sanha Kim[1,2], and A. John Hart[1]*

[1]Department of Mechanical Engineering, Massachusetts Institute of Technology, Cambridge, MA 02139, USA.

[2]Department of Mechanical Engineering, Korea Advanced Institute of Science and Technology, Daejeon 34141, South Korea.

*Corresponding author: ajhart@mit.edu

Abstract

Flexographic printing, which involves high-speed contact of an inked stamp against a substrate, is of increasing interest for scalable manufacturing of electronics in new formats. However, the adaptation of flexography to thinner, finer features generally required for printed electronics requires improved understanding of stamp-substrate contact mechanics. Here, we present a desktop plate-to-roll (P2R) printing apparatus which enables the study of flexographic printing in a semi-continuous format that mimics industrial printing. In particular, we tailor the specifications of the machine to use nanoporous stamps which were recently shown to enable printing of micron-scale ink features. Printing with nanoporous stamps requires precise control of stamp-substrate contact force (2-250mN) and elimination of shear force at the interface among others; these are accomplished using a flexure-supported substrate, and by coordinated rotary-linear motion of the system. We detail the design and evaluation of the P2R machine and demonstrate printing of high-resolution features (<3μm line width) with nanoporous stamps at speeds of up to 0.2 m/s.

1. Introduction

Flexographic printing uses molded rubber stamps for high-speed printing of graphics, and is now evolving into a next-generation electronics manufacturing process, for applications including large-area displays and smart packaging[1–3]. Using flexographic, inkjet, and other printing technologies, it is possible to print functional colloidal inks (e.g., conducting, semiconducting, dielectric) on glass, polymer, and paper substrates[2–14]. Therefore, the vision toward cost-effective production of printed electronics is to leverage the high-speed capability of traditional printing technologies, with adaptation to print electronically functional inks[4,9]. However, because printing of electronics requires much higher resolution and precision than printing of graphics[11,14], innovations in the printing processes and equipment are necessary to meet the resolution demands of the printed electronics industry[15]. This is most widely recognized within industry as a need for high-speed (>1 m/s), high-resolution (feature size <10 μm) printing [16–18]

To realize micron-resolution flexographic printing[18], we previously introduced a nanoporous stamping tool that printed significantly finer printed feature dimensions than traditional non-porous polymer stamps used in flexography. Importantly, nanoporous stamps can retain the ink within their volume, enabling the printed pattern to precisely replicate the shape of stamp features without suffering the squeeze-out and dewetting instabilities that occur when approaching such fine resolution using elastomer stamps. We realized nanoporous stamps comprising polymer-coated vertically aligned carbon nanotubes (CNTs) and demonstrated flexographic printing of diverse micrometer-scale patterns of a variety of functional nanoparticles inks including Ag, ZnO, WO_3, CdSe/ZnS. In addition, we showed that patterned transparent electrodes with ~3 μm feature size can be printed at a speed of 0.2 m/s, indicating promise for industrial use[19].

Laboratory development of high-resolution flexography, such as that achieved using the nanoporous CNT stamps, requires printing equipment with specific requirements on process parameters. A first requirement is the precise control of stamp-substrate contact force (2-250mN), as a threshold contact pressure must be reached to achieve the high fidelity print enabled by conformal nanomechanical stamp-substrate contact, yet the pressure must not exceed the value at which the stamp features buckle[18,19]. A second requirement is the control of shear force during contact, as the adhesive strength between the vertically aligned CNTs and the substrate is relatively weak, and therefore friction-driven roll contact cannot be used[20–24]. Third, the stamp-substrate alignment along the moving contact line must be maintained so that the contact force stays within the prescribed range enabling complete pattern transfer across the stamp area; for instance, misalignment of 42.4 arc seconds in the pitch or yaw directions will lead to a contact force error of 1mN.

In this paper, we report a desktop plate-to-roll (P2R) machine (Fig.1) which is designed and constructed to study advanced flexography techniques toward high-resolution and high-speed manufacturing of electronics. The machine is designed to investigate the relationship between process variables (e.g., contact force, printing speed) and the resulting quality, and to fabricate prototype patterns by printing of colloidal inks. The design details particularly consider the requirements for flexography using CNT-based nanoporous stamps; however the machine, and its design principles may be applied to other contact-based printing techniques.

2. Design of the plate to roll apparatus

The P2R machine (Fig. 2) achieves printing by synchronized rotary-linear motion of a roller over the printing stamp, which is fixed to a suspended platform supported by beam flexures. The machine accommodates stamps up to 20 x 20 mm in size, fixed to the substrate, and the roller can hold flexible substrates (wrapped thereon) up to 25 mm width. In this section, we explain the key design considerations of the four sub-systems - the flexure assembly, roller assembly, motion system, and the contact alignment system – which allowed us to achieve the necessary control of the contact force, contact speed, and alignment between the stamp and the substrate across the contact line.

2.1 Flexure Assembly

The flexure assembly supports the stamp, and enables control of the printing pressure by pre-calibration of its force-displacement relationship and control of the amount of interference between the roller and stamp during printing. For the P2R printing process, we assume that the roller and stamp coincide in line contact, and that the contact pressure will exhibit a Hertzian distribution (Fig. 3A). Therefore, the maximum pressure p_{max} can be determined by the applied force F, roller diameter R, and material properties of the stamp as [25]

$$p_{max} = \left(\frac{FE^*}{\pi R l}\right)^{1/2} \qquad [1]$$

where l is the length of the line contact and E^* is the reduced modulus between the contacting materials 1 (roller with receiving substrate attached) and 2 (stamp) given by their Young's moduli and Poisson's ratios as

$$\mathrm{E}^* = \left(\frac{1-\upsilon_1^2}{E_1} + \frac{1-\upsilon_2^2}{E_2}\right)^{-1} \qquad [2]$$

The CNT stamp is assumed to have linear elastic behavior within the strain levels reached under the applied contact pressure required for uniform ink transfer[19]. In previous work, we showed that uniform ink transfer from a CNT microstructure to a solid substrate can be achieved when the contact pressure ranges from 28-150 kPa[18,19]. We control the contact pressure by the force exerted through a flexure assembly (Fig. 3B, C). Using Eq. [1], we determine that the aforementioned contact pressure range is equivalent to an applied force of 2-250 mN for ~20 mm line contact (Fig. 3D); this value is directly proportional to the stamp width. By making the flexure at least 50-fold more compliant than CNT stamps (stiffness = 10-100 kN/m), the contact force between the plate and the roller can be determined solely by the flexure stiffness and deflection. That is, for a known flexure stiffness, we can control the flexure deflection and hence the contact force and pressure. For example, a deflection of 10 microns will correspond to the minimum force of 2 mN.

We designed an aluminum flexure with a known stiffness (243.3 N/m) which allows us to apply the required force by varying the deflection (Fig. 3B-D). The first resonant frequency of the flexure (108.52 Hz, see Figure S1 in Supporting Information) is much greater than both the rotational speed (1.27Hz) used in the printing experiments and the maximum motor speed (2.23Hz). Therefore, we conclude that resonant vibration of the flexure is not a concern with respect to control of the printing force. A capacitance probe (Lion Precision, C8-2.0-2.0, resolution 2.1 nm [26]) placed between the flexure holder and the flexure is used to measure the deflection (Fig. 3C).

2.2 Roller Assembly

It was necessary for the roller assembly to have stiffness, and total indicated runout, that met the requirements for force application and displacement control mentioned above. The roller is made of aluminum (Al6061), and the roller assembly consists of the roller, shaft, angular contact bearings, and the bearing housing. The nominal design is an aluminum roller of 50 mm diameter. The roller is mounted at the end of a stepped shaft supported by two angular contact bearings (ABEC-7) assembled in a back-to-back configuration. By placing the roller adjacent to the supporting bearings and assembling the bearings in back-to-back configuration, we achieved a high moment stiffness and therefore ensured low shaft deflections due to dynamic loading.

The roller was mounted to the bearings using a shrink fit. The roller shaft was cooled, then the bearings were pressed on the shaft. Then, the bearing housing was heated and the roller shaft with bearings was pressed to form the roller assembly. A locknut and lockwasher at the shaft end were used to preload the angular contact bearing. Yet, as assembled, the runout of the roller was measured to be 25 μm; therefore, to reduce the runout, the roller surface was ground after assembly (Fig. 4A), giving a total indicated run out of 5 μm after grinding (Fig. 4B). A 5 μm total indicated run out will cause the contact force to change by 1 mN; this falls well within the pressure range prescribed for uniform printing. In addition, the design allows easy exchange of rollers with different diameters, lengths and materials when needed. However, after assembling a new roller surface grinding must be performed to achieve the runout specification.

2.3 Motion System

To enable P2R printing, we constructed a synchronized rotation-translation system that achieves slip-free motion of the roller over the stamp (which is attached to the flexure). Slip-free rolling contact can be achieved by driving the rotor about the rotary axis (ω) and letting the interfacial friction provide the linear motion (V) of the stamp, or by driving the stamp along the linear axis (V) and letting the friction provide the rotary motion (ω) of the roller. However, the CNT stamps cannot endure the shear stress induced by the friction due to their own mechanics and the limited adhesion between CNT microstructures and their base substrate[20–24]. To overcome this limitation, the P2R system has independent drives for the roller rotation and translation, with motion synchronized such that $R\omega=V$.

To provide smooth rotary motion for the roller, a slotless, brushless DC motor (Aerotech, BMS60) is used [27]. The motor has a built-in rotary encoder, and the position resolution of the roller along the circumference is 39 nm. A linear motor (Aerotech, ANT 130L) with 160 mm travel range, 5 nm resolution, and 350 mm/sec speed limit is used to translate the roller assembly[28]. With these two motors, velocity control can be implemented to eliminate slip and achieve smooth motion at speeds ranging from <1mm/sec to >100 mm/sec (see Table S1 in Supporting Information). Two networked PWM digital controllers (Aerotech, ENSEMBLEMP10-IO-MXU) are used to control the two motors and synchronize their motions[29].

Fig. 5 shows the block diagram of the closed-loop control system. The transfer functions of the plant and controller are $P(z)$ and $C(z)$, respectively. For the rotary motion, the plant consists of the dynamic system including the BMS60 motor, coupling, shaft and roller. For the linear motion, the plant consists of the ANT130 L motor and the roller assembly mounted on the motor. The closed loop transfer function is given by

$$\frac{Y}{X} = \frac{FF(z)F(z)P(z) + C(z)F(z)P(z)}{1 + C(z)F(z)P(z)} \quad [3]$$

where the transfer functions of the filter and feedforward controller are *F(z)* and *FF(z)* respectively. Fig. 6 shows the measured open loop and closed transfer functions of the rotary and linear motion dynamic systems. For the rotary motion system, cross over frequency is 82.7 Hz and the phase margin at this frequency is -163.7^0. For the linear motion system, cross over frequency is 56.9 Hz and the phase margin at this frequency is -151.9^0. The phase is not equal to -180^0 across the entire frequency range indicating infinite gain margin. These high margins render the rotary and linear motion systems stable, and able to track trajectories and hence eliminate slip between rotary and linear motions.

2.4 Contact Alignment System

It is also necessary to ensure that the contact pressure is uniform across the contact line, and, as much as possible, throughout the travel of the roller while contacting the stamp (Fig. 7A). This was achieved by fine adjustment of the pitch and yaw orientation of the flexure stage, while measuring the forces using strain gauges bonded to the four legs of the flexure (Fig. 7B,C). The pitch-yaw stage (ThorLabs, PY003, resolution = 109.1 arc seconds) was placed on top of the Z motion stage. The alignment was deemed to be complete when the contact pressure during the printing cycle stays within the desired range. With good alignment, pairs of strain gages attached in the locations "S1 and S2" and "S3 and S4" in Fig. 7B, should have the same output during the printing cycle as shown in Fig. 7C.

The total error in printing force due to misalignment, flatness and shaft runout is estimated to be 6.6 mN; calculations are given in the SI. This is comparable to the printing force at the lower end of the range (2mN), but much less than that at the higher end of the range (250mN). Fig. 8 shows the measured force during printing at print speeds of 1, 18 and 100 mm/sec. The nominal (target) printing force is 18.2 mN in these experiments and the measured printing force has maximum values of 10.2, 25.7, and 17.7 mN at print speeds of 1, 18 and 100 mm/sec, respectively. The force variation during a printing cycle and between experiments can be attributed to flatness, shaft runout, and surface variations due to PET film affixed to the roller for each experiment.

3. Plate-to-Roll Printing Experiments

3.1 Experimental Procedure

Nanoporous stamps are fabricated by chemical vapor deposition (CVD) growth of CNT forests from a lithographically patterned catalyst film on a silicon wafer[18]. Fig. 9A shows SEM images of the nanoporous stamp with an array of cylindrical micropillars 100 μm in diameter and 130 μm in spacing between their centers.

The mechanical compliance, surface roughness, and wettability of the stamp structures are tailored via plasma treatment of the CNTs and subsequent coating with a thin layer of polymer (pPFDA, 20 nm) by initiated chemical vapor deposition (iCVD)[18,30,31]. To prepare the stamp for printing, a 100 μl droplet of colloidal silver nanoparticle ink (Sigma Aldrich, <10 nm in tetradecane, 50-60 wt%) is pipetted onto the stamp. Then, excess ink is removed in two steps: first, the stamp is spun at 1500 rpm for 1-3 minutes; then,

the wet stamp is brought into contact with a uniform CNT forest, as described in our previous work[18]. After the removal of excess ink, ink wets the stamp microstructures conformally[19].

P2R printing experiments are conducted as follows. First, a strip of 100 μm thick PET film (average roughness, ~6-10nm; McMaster-Carr) is attached to the roller, and the printing stamp is placed on the flexure and brought into contact with the roller at approximately the midpoint between the two ends of the stamp. Next, we apply a contact force of ~25 mN by displacing the flexure vertically and monitoring the deflection via the capacitance probe signal (Fig. 8). The pattern density also influences the target force and hence the flexure deflection. Next, we detach the stamp from the flexure, apply the ink on the stamp and remove the excess ink as outlined in section 3.1. Then, we attach the wet stamp to the flexure using an adhesive tape. Last, we command the motors to execute the printing step. We provide videos showing the motion of the system through for printing speeds of 2, 20, and 200 mm/s (Videos S1-S3 in Supporting Information). The printing process is repeated by removing the printed PET film from the roller and attaching a new film; 10-15 prints are completed without re-inking the stamp.

3.2 High resolution P2R printing by force control with no slip at various speeds

Using the newly built P2R apparatus, we demonstrate printing of precise patterns of isolated features (from cylindrical micropillars array stamps, 100μm diameter), as well as connected features (honeycomb stamp patterns). Fig. 9B shows the optical microscope image of the printed circle (from micropillar stamp) patterns on PET substrates at printing speeds of 1, 18, and 100 mm/s, which show high fidelity without distortion due to the application of controlled contact force without slip (see Supporting information). The mean and standard deviation of the diameters and center to center distances measured from the printed patterns (Fig. 9B) are summarized in Table 1. The lateral error, defined as the difference between the lateral dimension of the printed layer and that of the stamp pattern, is a major consideration for precision printing. The dimensions are measured by optical microscopy of the stamp before inking, and of the printed pattern; for each reported dimension, five micropillars and features were averaged, respectively.

Speed (mm/sec)	**Print Force (mN)**	**Diameter Mean ± Stdev (μm)**	**Center-center distance Mean ± Stdev (μm)**
1	9.3	100.3 ±1.6	130.5±0.6
18	25	105.5±2.4	131.4±0.5
100	15.6	99.8±1.9	131.3±1.1

Table 1: The mean and standard deviation of the diameters and center to center distances measured from the printed micropillar patterns (see Figure S2 and Table S2 in Supporting information)

In Fig. 10A and B, we show the microscope images of stamp with a honeycomb pattern with a line width of 3 microns, and the printed pattern on flexible glass[32] (SCHOTT, Thin Glass AF32) at 100 mm/sec . The stamp pattern has circular holes but the printed pattern has hexagons and this is likely due to capillary densification of the stamp upon inking [33,34]. The honeycomb patterns are of significance to manufacture transparent conductive films such as those used in photovoltaics and touchscreen displays[35–37].

From the printed patterns, four hexagons located at the corners and one in the centroid of a square were chosen for analysis (Fig. 10B). The width values of the five hexagons and their center-center distances are

13.0±1.0μm and 132.7±0.3μm, respectively. We also confirm that the dimensions are invariant with print speed and direction, yet, statistical analysis of the dimensions of additional features and groups of features spanning large areas will be necessary to establish a confidence interval. The surface profile (Fig. 10C) of the printed honeycomb pattern was measured using a laser scanning confocal microscope (Keyence Model VK-X250), and the thickness profiles perpendicular to the sides are presented in Fig. 10D. The mean and standard deviation of the thicknesses measured along the lines 1-6 are 43.8±11.3 nm, with a RMS roughness of 1.1 nm except at the corners where the sides meet. These values were calculated from thickness profiles at three locations on each side of a hexagon (see Figure S3, S4 and Table S3 in Supporting Information)

Among the sides, though the feature width (~1.6μm) is uniform, the thickness profiles show non-uniformity, significant variation (~11nm) and accumulation of ink at the corners. These imperfections can be attributed to stamp height variation and non-uniform ink distribution in the different stamp regions. The printed patterns would need to be sintered to be rendered electrically conductive, either by flash sintering or thermal annealing. In prior work using manual plate-to-plate printing with nanoporous stamps, we printed silver honeycomb patterns with 94% transparency and thermally annealed them to achieve a sheet resistance of 3.6 ohm/sq [18] which compares favorably to state-of-the-art transparent conductive films and patterned metal films.

Discussion

The desktop P2R apparatus provides a convenient, precise means to study flexographic printing processes and to develop new stamps, to study process parameters, and to prototype patterns and (in the future) multilayer devices from various colloidal inks. The compact setup is particularly suitable to conduct experimental studies by varying print speed, contact force, and ink-substrate materials and interactions (e.g., wettability). In addition, it allows state-of-the-art micro- and nanofabrication techniques to be used to prototype new stamp designs, including but not limited to the present case study of CNT-based nanoporous stamps. A comparison of the specifications of the P2R system with other laboratory scale P2R and R2R printing equipments is summarized in Table S4 (refer Supporting information)[38–40]. Furthermore, in our earlier work, we show a comparison of the print resolution and speed of nanoporous flexographic printing with other industrial printing processes[18].

Reflecting on our achievements with the P2R system, we can consider a potential pathway toward a continuous roll-to-roll (R2R) printing system using a nanoporous stamp roll. We present a conceptual design for a continuous R2R printing machine in Fig. 11, consisting of a nanoporous stamp roller, an anilox roller for inking, and the supporting roller to support the target substrate. Nanoporous stamp rollers can be fabricated by synthesizing the CNT forests on a flexible substrate such as ultraflat thin copper foils that can be wrapped on a rigid roller, while a non-patterned CNT forest can be used as the anilox roller. Although silicon and quartz are advantageous as substrate materials due to their inert characteristics and mechanical rigidity, copper has been widely studied as a growth substrate owing to its cost and mechanical flexibility.[41,42] The anilox roller coating must have sufficient stiffness to withstand the forces applied by the doctor blade used to distribute on the roller; this can achieved by reinforcing the CNTs with a ceramic such as aluminum oxide (e.g., by atomic layer deposition [43]) while maintaining porosity and wettability[44].

In the conceptual R2R machine, the bearings supporting the stamp roller and the substrate rollers can be assembled on movable supports that are attached to XY double parallelogram flexure mechanisms[40,45–

47]. The motion stage holding the bearings can be displaced with an actuator causing the stamp roller to contact the substrate with a prescribed force. The alignment between the stamp and substrate rollers can be controlled by using the actuators and the flexures because, unlike the P2R machine, the contact line is fixed in the R2R machine. The flexure beams can be instrumented with strain gages and the strains can be used to measure the misalignment and correct it by displacing the respective actuators by prescribed displacements, possibly with real-time feedback to account for run-out of the rollers. Additionally, the motors driving each of the three rollers must be independently driven and synchronized so as to provide slip-free smooth motion at each of the interfaces.

4. Conclusion

We designed and fabricated a plate to roll (P2R) printing apparatus for benchtop study of flexographic printing with precision control. Using nanoporous stamps, we conducted printing experiments by controlling the contact force and speed. The lateral dimensions and the thickness of the printed features show that the machine meets the functional requirements including control of contact force, alignment, and slip between the stamp and substrate. In addition, the P2R apparatus can be adequate for testing versatile substrate combinations, including both rigid-to-flexible and flexible-to-flexible configurations. Therewith, findings from lab-scale P2R printing can guide strategies for scale-up using established, or new, industrial roll-to-roll printing equipment.

Acknowledgements

Financial support was provided by the National Science Foundation (CMMI-1463344, CMMI-1826216), the MIT Energy Initiative Seed Fund, and the MIT-Skoltech Next Generation Program. We thank Prof. David Trumper for advice on the design of the motion system; Steve Malone, Jun Young Yoon and Stuart Baker for assistance in motor selection; Mark Belanger, Patrick McAtamney and the MIT Edgerton Center for fabrication support; Hangbo Zhao for performing catalyst deposition and patterning; and Hossein Sojoudi and Prof. Karen Gleason for assistance in polymer coating. We also thank Ulrich Peuchert, David Asch, Matthias Jotz, and David Vanderpool from SCHOTT for providing the flexible glass samples. CNT catalyst deposition and patterning were performed at the MIT Microsystems Technology Laboratory (MTL). Electron microscopy and profilometry were performed at the shared experimental facilities at the MIT Center for Materials Science and Engineering (CMSE) supported in part by the MRSEC Program of the National Science Foundation under award number DMR-1419807. Confocal microscopy was performed at the Institute for Soldier Nanotechnologies at MIT supported in part by the U.S. Army Research Office under Cooperative Agreement Number W911NF-18-2-0048.

References

[1] Darhuber AA, Troian SM, Wagner S. Physical mechanisms governing pattern fidelity in microscale offset printing. J Appl Phys 2001;90:3602–9.

[2] Lloyd JS, Fung CM, Deganello D, Wang RJ, Maffeis TGG, Lau SP, et al. Flexographic printing-assisted fabrication of ZnO nanowire devices. Nanotechnology 2013;24:195602.

[3] Vena A, Perret E, Tedjini S, Tourtollet GEP, Delattre A, Garet F, et al. Design of chipless RFID tags printed on paper by flexography. IEEE Trans Antennas Propag 2013;61:5868–77.

[4] Alem S, Graddage N, Lu J, Kololuoma T, Movileanu R, Tao Y. Flexographic printing of polycarbazole-based inverted solar cells. Org Electron Physics, Mater Appl 2018;52:146–52.

[5] Mogg BT, Claypole T, Deganello D, Phillips C. Flexographic printing of ultra-thin semiconductor polymer layers. Transl Mater Res 2016;3:15001.

[6] Grubb PM, Mokhtari Koushyar F, Lenz T, Asghari A, Gan G, Xia W, et al. High Speed Roll-to-Roll Printable Transistor Enabled by a Pulsed Light Curable CNT Ink. J Manuf Mater Process 2019;3:33.

[7] Grau G, Cen J, Kang H, Kitsomboonloha R, Scheideler WJ, Subramanian V. Gravure-printed electronics: Recent progress in tooling development, understanding of printing physics, and realization of printed devices. Flex Print Electron 2016;1:23002.

[8] Ostfeld AE, Deckman I, Gaikwad AM, Lochner CM, Arias AC. Screen printed passive components for flexible power electronics. Sci Rep 2015;5:1–11.

[9] Valmiro R, Kitaguti H, Barbin SE. A silk-screen printed RFID tag antenna. Asia-Pacific Microw Conf Proceedings, APMC 2015;3:7–9.

[10] Lau PH, Takei K, Wang C, Ju Y, Kim J, Yu Z, et al. Fully Printed, High Performance Carbon Nanotube Thin-Film Transistors on Flexible Substrates. Nano Lett 2013;13:3864–9.

[11] Homenick CM, James R, Lopinski GP, Dunford J, Sun J, Park H, et al. Fully Printed and Encapsulated SWCNT-Based Thin Film Transistors via a Combination of R2R Gravure and Inkjet Printing. ACS Appl Mater Interfaces 2016;8:27900–10.

[12] Grubb PM, Subbaraman H, Park S, Akinwande D, Chen RT. Inkjet printing of high performance transistors with micron order chemically set gaps. Sci Rep 2017;7:1–8.

[13] Park J, Kim M, Yeom SW, Ha HJ, Song H, Min Jhon Y, et al. Flexible ambipolar organic field-effect transistors with reverse-offset-printed silver electrodes for a complementary inverter. Nanotechnology 2016;27:225302.

[14] Byun K, Subbaraman H, Lin X, Xu X, Chen RT. A 3μm channel, ink-jet printed CNT-TFT for phased array antenna applications. Proc. 2013 IEEE Texas Symp. Wirel. Microw. Circuits Syst. WMCS 2013, 2013.

[15] LOPEC 2016 – Printed electronics : A key technology of the future 2016:5–8.

[16] Khan S, Lorenzelli L, Dahiya RS. Technologies for printing sensors and electronics over large flexible substrates: A review. IEEE Sens J 2015;15:3164–85.

[17] Koo H, Lee W, Choi Y, Sun J, Bak J, Noh J. Scalability of carbon-nanotube- based thin film transistors for flexible electronic devices manufactured using an all roll- to-roll gravure printing system. Nat Publ Gr 2015:1–11.

[18] Kim S, Sojoudi H, Zhao H, Mariappan D, McKinley GH, Gleason KK, et al. Ultrathin high-resolution flexographic printing using nanoporous stamps. Sci Adv 2016;2:e1601660.

[19] Mariappan DD, Kim S, Boutilier MSH, Zhao J, Zhao H, Beroz J, et al. Dynamics of Liquid Transfer from Nanoporous Stamps in High-Resolution Flexographic Printing. Langmuir 2019;35:7659–71.

[20] Lahiri I, Lahiri D, Jin S, Agarwal A, Choi W. Carbon nanotubes: How strong is their bond with the substrate? ACS Nano 2011;5:780–7.

[21] Westover AS, Choi J, Cui K, Ishikawa T, Inoue T, Xiang R, et al. Load dependent frictional response of vertically aligned single-walled carbon nanotube films. Scr Mater 2016;125:63–7.

[22] Lahiri D, Benaduce AP, Kos L, Agarwal A. Quantification of carbon nanotube induced adhesion of osteoblast on hydroxyapatite using nano-scratch technique. Nanotechnology 2011;22:355703.

[23] Zhang Y, Suhir E, Xu Y, Gu C. Bonding strength of a carbon nanofiber array to its substrate. J Mater Res 2006;21:2922–6.

[24] Li Y, Zhang H, Yao Y, Li T, Zhang Y, Li Q, et al. Transfer of vertically aligned carbon nanotube arrays onto flexible substrates for gecko-inspired dry adhesive application. RSC Adv 2015;5:46749–59.

[25] Johnson KL. Contact Mechanics. Cambridge University Press; 1987.

[26] Lion Precision Capacitance Probe Manual n.d. http://www.lionprecision.com/capacitive-sensors/probes8mm.html.

[27] Aerotech Slotless Brushless Motor Manual n.d. https://www.aerotech.com/product-catalog/motors/rotary-motors/bms-series.aspx.

[28] Aerotech Linear Motion Stage Manual n.d. http://www.aerotech.com/product-catalog/stages/linear-stages/ant130-l.aspx.

[29] Aerotech Ensemble MP Controller Manual n.d. https://www.aerotech.com/product-catalog/drives-and-drive-racks/ensemble-mp.aspx.

[30] Gupta M, Gleason KK. Initiated chemical vapor deposition of poly(1H,1H,2H,2H-perfluorodecyl acrylate) thin films. Langmuir 2006;22:10047–52.

[31] Sojoudi H, Kim S, Zhao H, Annavarapu RK, Mariappan D, Hart AJ, et al. Stable Wettability Control of Nanoporous Microstructures by iCVD Coating of Carbon Nanotubes. ACS Appl Mater Interfaces 2017;9:43287–99.

[32] Schott Thin Glass AF 32 - Manual n.d. https://www.schott.com/d/advanced_optics/5b420dd5-2a84-4c81-98e4-9efdcc011e61/1.3/schott-af-32-eco-thin-glass-may-2013-eng.pdf.

[33] Volder M De, Hart AJ. Engineering Hierarchical Nanostructures by Elastocapillary Self-Assembly. Angew Chemie Int Ed 2013;52:2412–25. doi:10.1002/anie.201205944.

[34] Volder M De, Tawfick SH, Park SJ, Copic D, Zhao Z, Lu W, et al. Diverse 3D Microarchitectures Made by Capillary Forming of Carbon Nanotubes. Adv Mater 2010;22:4384–9.

[35] Van De Groep J, Spinelli P, Polman A. Transparent conducting silver nanowire networks. Nano Lett 2012;12:3138–44.

[36] Linnet J, WAlther AR, Wolff C, Albrektsen O, Mortensen NA, Hansen K. Transparent and conductive electrodes by large-scale nano-structuring of noble metal thin-films. Opt Mater Express 2018;8:1733–46.

[37] Catrysse PB, Fan S. Nanopatterned metallic films for use as transparent conductive electrodes in optoelectronic devices. Nano Lett 2010;10:2944–9.

[38] Zhou X, Wang D, Wang J, Chen SC. Precision design and control of a flexure-based roll-to-roll

printing system. Precis Eng 2016;45:332–41. doi:10.1016/j.precisioneng.2016.03.010.

[39] Choi YM, Kang D, Lim S, Lee MG, Lee SH. High-Precision Printing Force Control System for Roll-to-Roll Manufacturing. IEEE/ASME Trans Mechatronics 2017;22:2351–8.

[40] Petrzelka JE, Hale MR, Hardt DE. Contact pattern sensitivity and precision machine control in roll-to-roll microcontact printing. MRS Symp. Proc., vol. 1529, 2013.

[41] Zhong G, Yang J, Sugime H, Rao R, Zhao J, Liu D, et al. Growth of high quality, high density single-walled carbon nanotube forests on copper foils. Carbon N Y 2016;98:624–32.

[42] Wang H, Feng J, Hu X, Ng KM. Synthesis of aligned carbon nanotubes on double-sided metallic substrate by chemical vapor deposition. J Phys Chem C 2007;111:12617–24.

[43] Brieland-shoultz A, Tawfick S, Park SJ, Bedewy M, Maschmann MR, Baur JW, et al. Scaling the Stiffness , Strength , and Toughness of Ceramic- Coated Nanotube Foams into the Structural Regime. Adv Funct Mater 2014;24:5728–35.

[44] Zhao H, Jacob C, Stone HA, Hart AJ. Liquid Imbibition in Ceramic-Coated Carbon Nanotube Films. Langmuir 2016;32:12686–92.

[45] Awtar S. [*Dissertation*] Synthesis and analysis of parallel Kinematic XY flexure mechanisms. Massachusetts Inst Technology; 2004.

[46] Awtar S, Slocum AH. Constraint-Based Design of Parallel Kinematic XY Flexure Mechanisms. J Mech Des 2007;129:816.

[47] Li C, Chen SC. A Flexure-based Multi-layer Roll-to-roll Printing System. Proc. - 32nd ASPE Annu. Meet., 2017, p. 393–7.

FIGURES

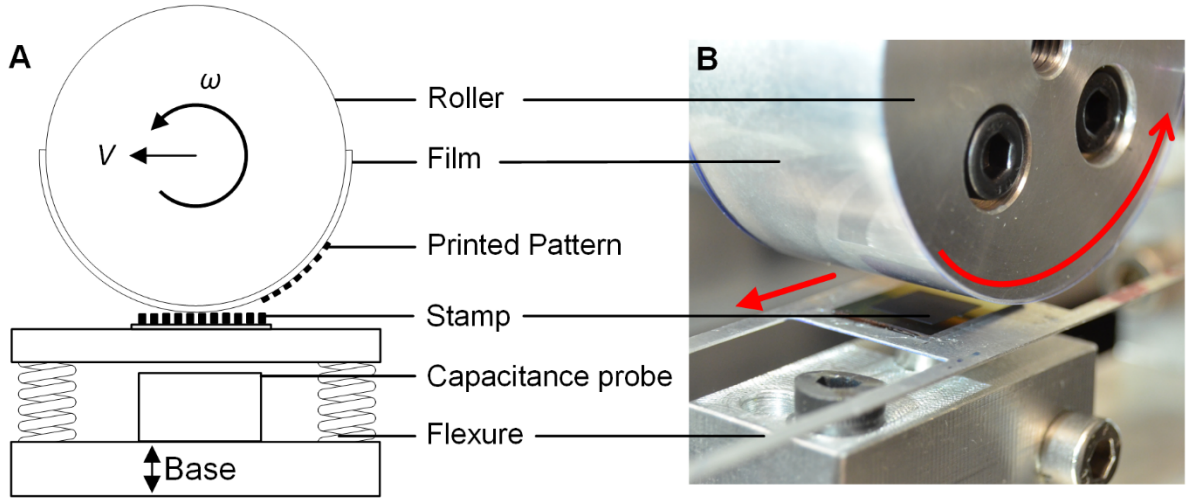

Figure 1: A desktop plate to roll apparatus with slip-free smooth rotary and translation motions, adjustable contact force and alignment control for high-resolution printing applications A) Schematic and B) Photograph of the machine showing the printing stamp, flexible substrate, flexure used for setting the contact force, displacement sensor and the roller.

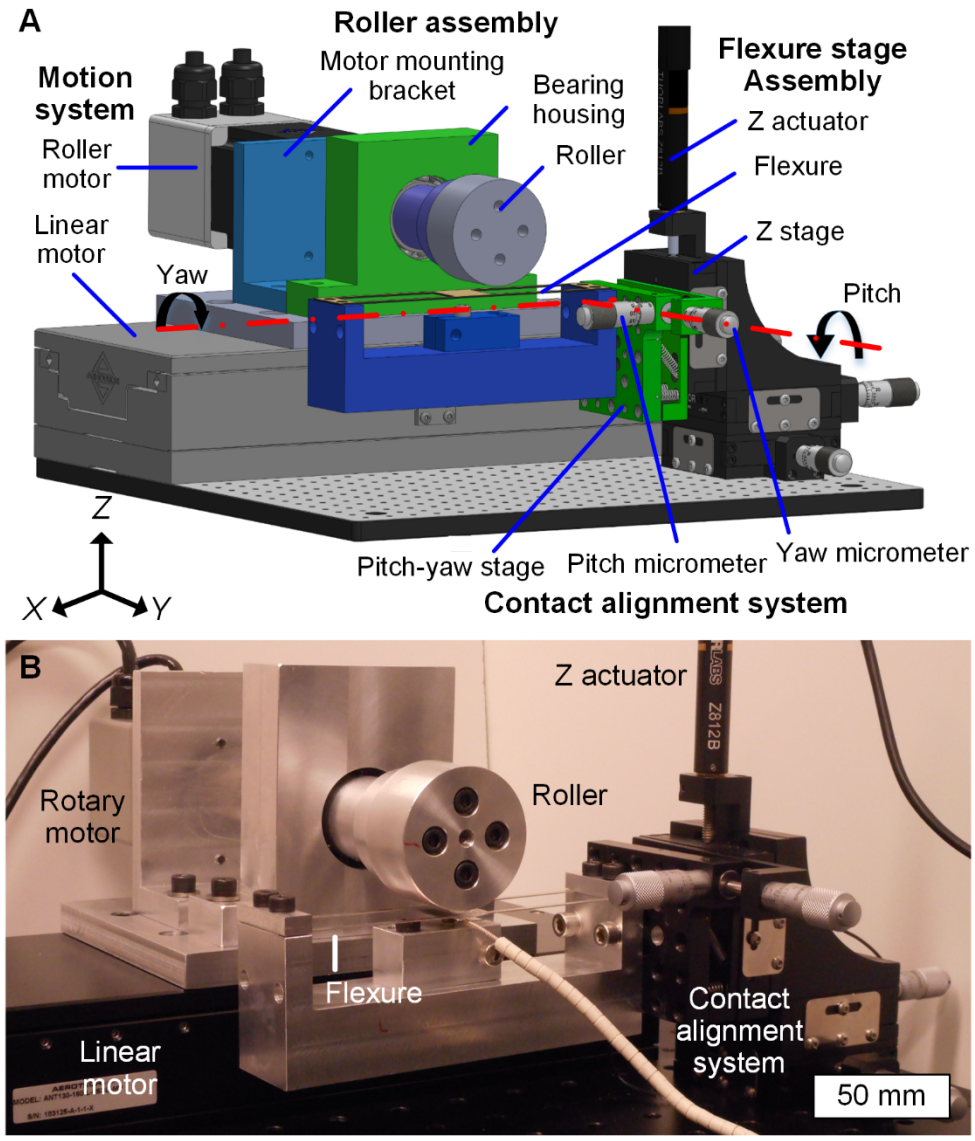

426

427 **Figure 2:** CAD model of the plate to roll machine A) Schematic and B) Photograph of the machine
428 showing the four subsystems including roller assembly, stage assembly, motion and the contact
429 alignment systems

430

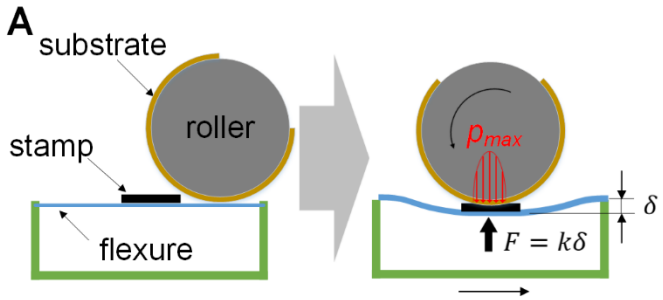
A
substrate
roller
stamp
flexure
p_{max}
δ
$F = k\delta$


B

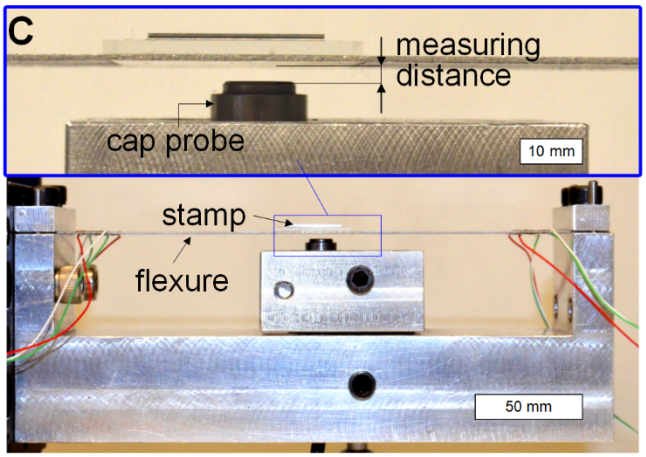
C
measuring
distance
cap probe
10 mm
stamp
flexure
50 mm

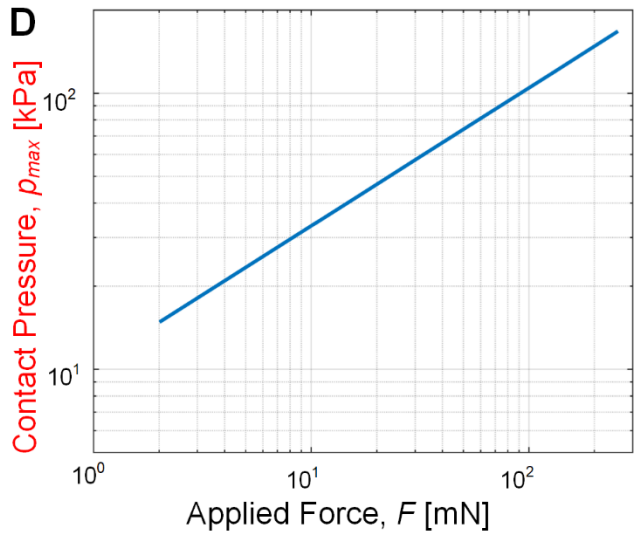
D
Contact Pressure, p_{max} [kPa]
10^2
10^1
10^0
10^1
10^2
Applied Force, F [mN]

431

Figure 3: A Flexure, capacitance based displacement sensor and a micrometer stage are used to set the contact force between the plate and the roller A) Schematic and B) Photograph of the flexure C) photograph showing the method of application of contact force via a flexure, displacement sensor and Z motion of a rigid flexure holder D) Relationship between the contact pressure and applied force based on the cylinder-plane Hertzian contact mechanics modeling

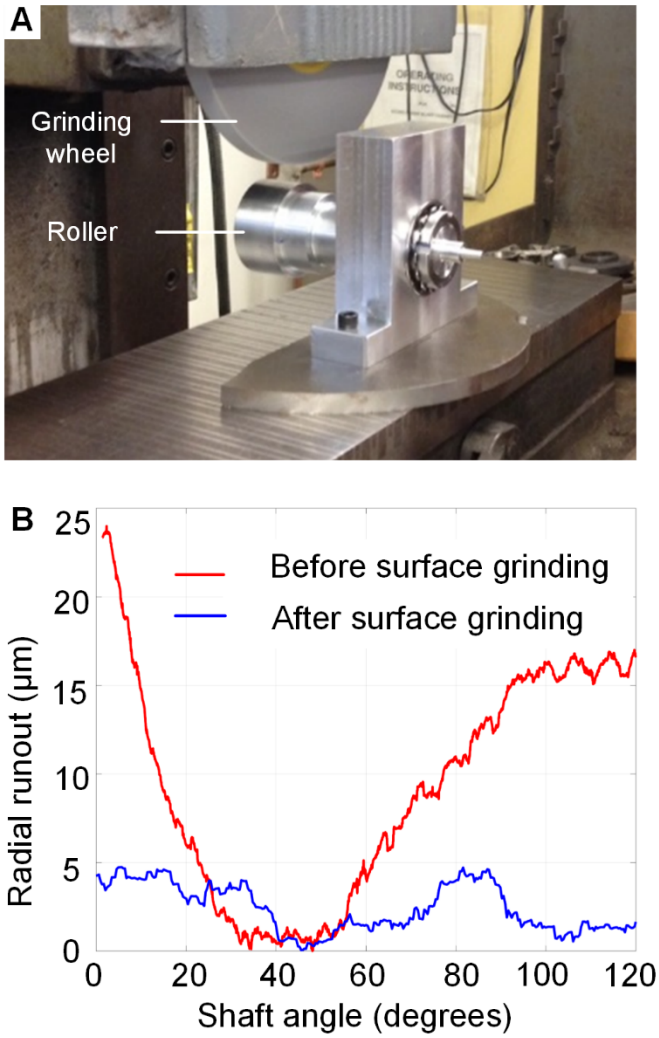

Figure 4: Surface grinding of the roller A) Photograph shows the surface grinding wheel and the roller as part of the roller assembly after surface grinding B) Radial runout measurements of the shaft show the reduction in radial runout after surface grinding to less than 5 microns, keeping the force variations during printing to within 1.2mN

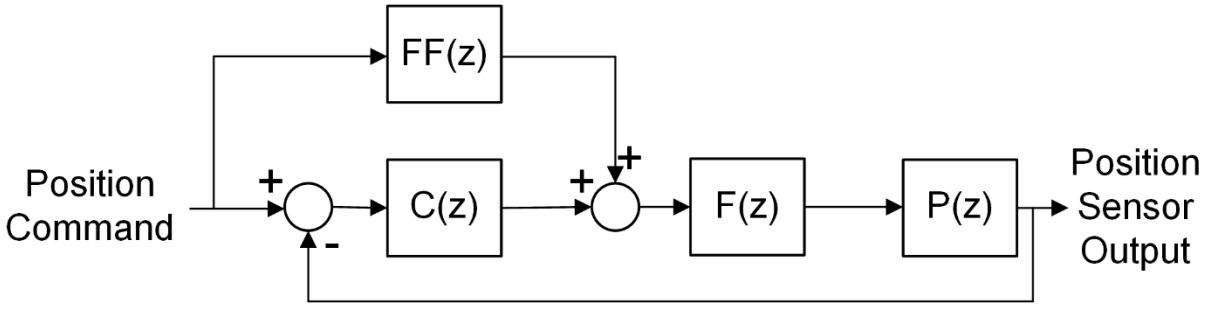

Figure 5: Roller and linear motion stages use tuned feedforward and PID controllers to achieve smooth motion (*P(z)* , *C(z)*, *FF(z)*, and *F(z)* are the transfer functions of the plant, PID controller feedforward controller, and servofilters respectively)

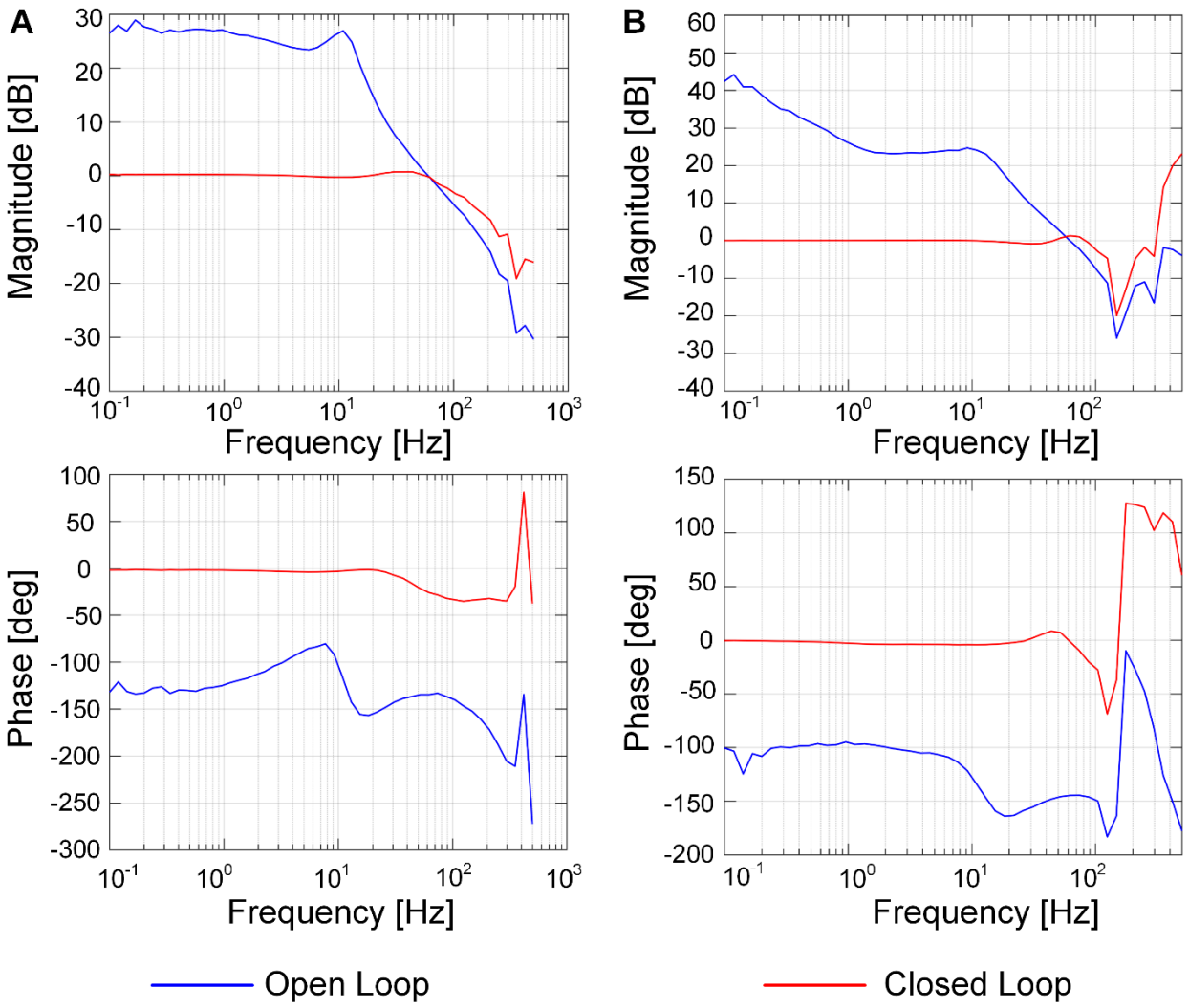

Figure 6: Closed loop frequency response measurements of A) the linear motion stage and B) the roller show a stable dynamic system with flat amplitude response for frequency up to 20 Hz and sufficient phase and gain margins

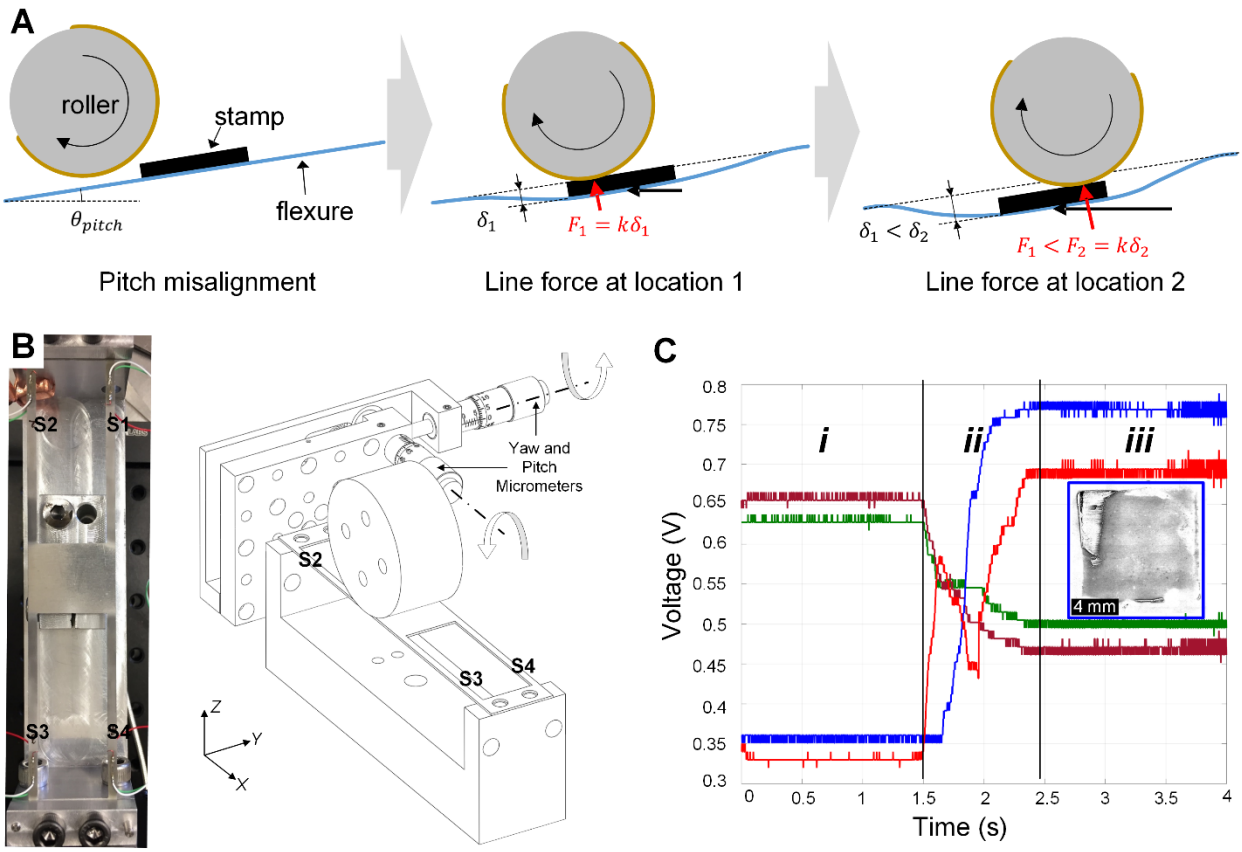

Figure 7: Pitch-yaw micrometer stages are used to align the roller and plate during printing, based on readings from strain gages attached to the beams in the flexure stage. A) Schematics showing the force variation during roll printing when flexure is misaligned. B) Photograph and CAD model showing the pitch yaw stage, micrometers, roller, flexure holder, flexure and the locations of the strain gages S_1, S_2, S_3, and S_4. C) Exemplary values of the strain gages S_1, S_2, S_3 and S_4 at the start (*i*), during printing (*ii*) and stop of printing (*iii*) in terms of the amplified voltages.

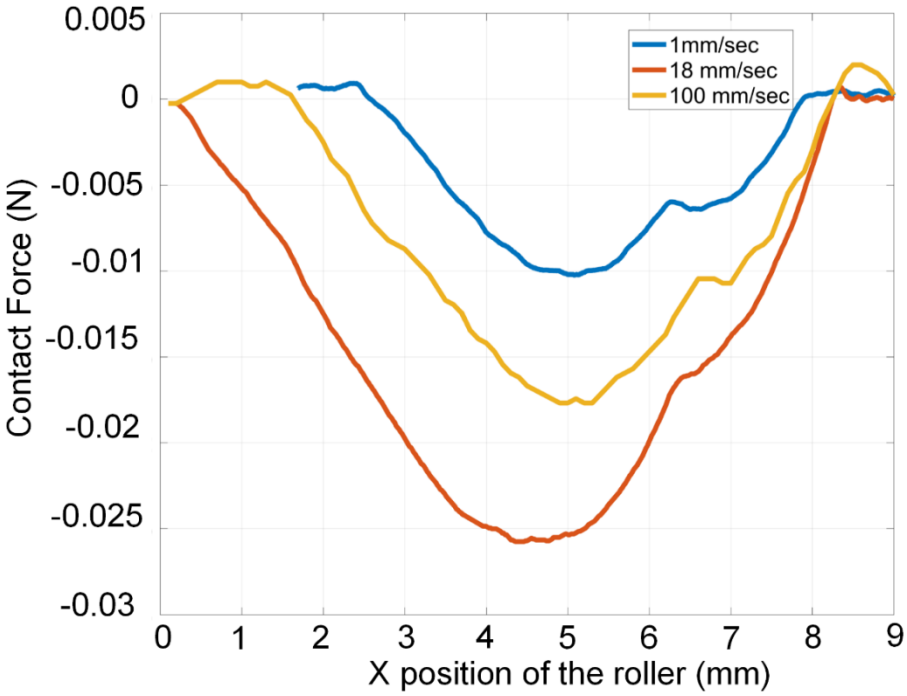

474

475 **Figure 8:** Printing force variation during printing at low, intermediate, and high speeds.

476

477

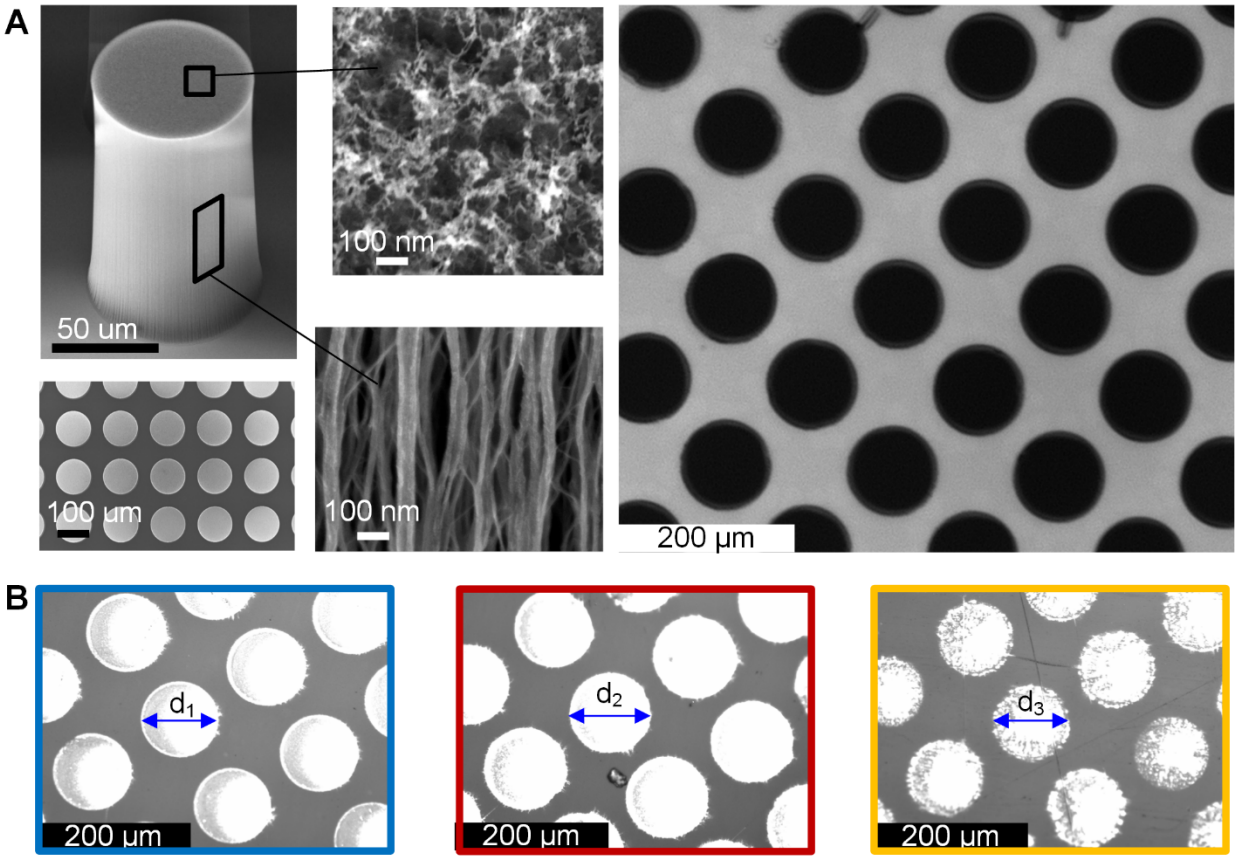

Figure 9: Nanoporous Printing Stamp, Printed Patterns and the Printing Force A) SEM image of the micropillar in the printing stamp, nanoscale pore shown on the top surface and the sidewalls of the micropillar and the optical image of the printing stamp B) Microscope image of printed patterns at low (1 mm/sec), intermediate (18 mm/sec) and high speeds (100 mm/sec)

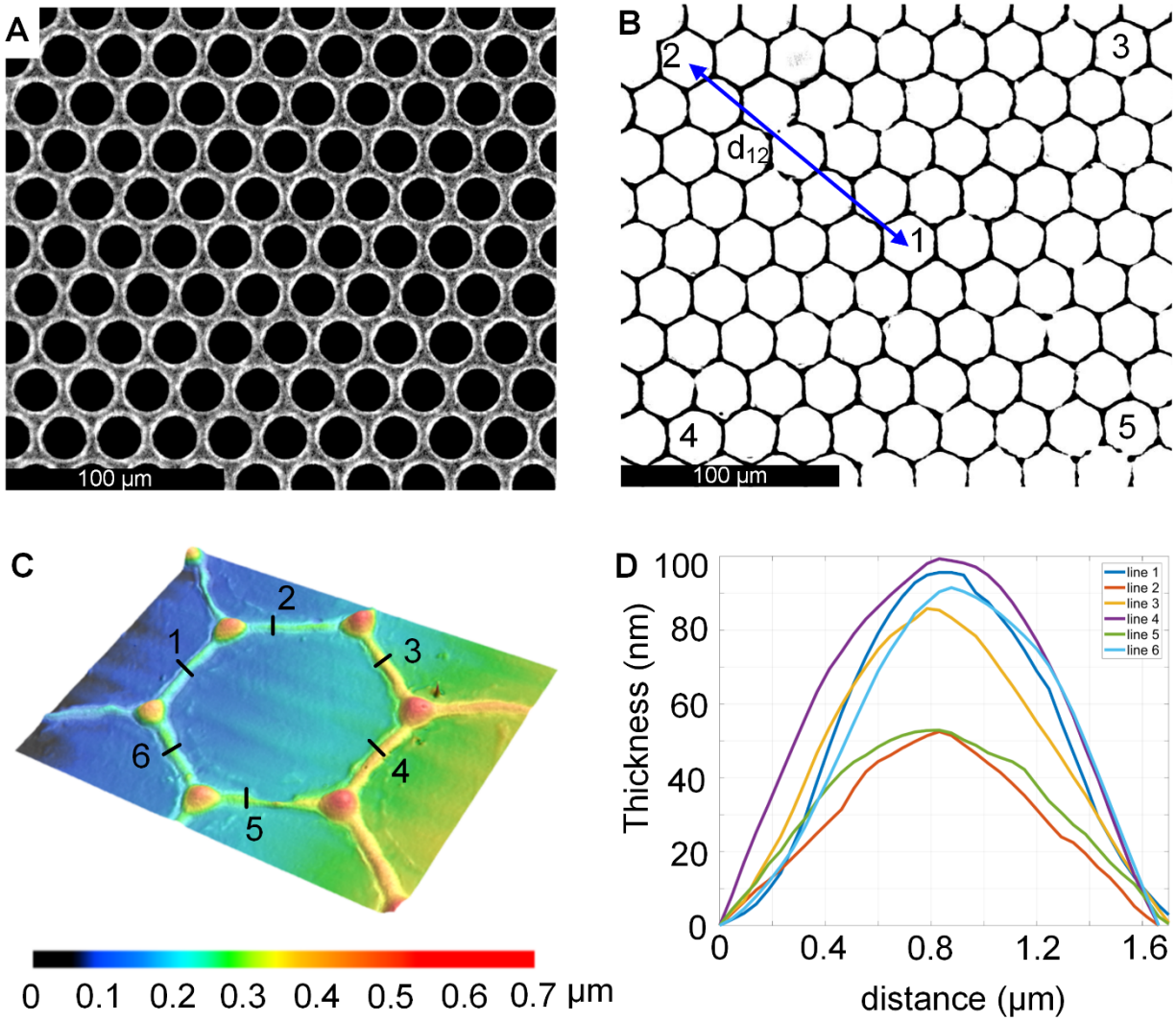

Figure 10: Printing of high resolution honeycomb patterns at 100 mm/sec. A) Optical microscope image of stamp shows a honeycomb stamp consisting of hexagons with line width of 2 microns B) Printed pattern – sides of the hexagons and the center-center distances of the hexagons have a standard deviation of 1 and 0.26 microns respectively C) Laser scanning confocal microscope image of one of the hexagons in the printed pattern D) Measured profile of the sides of the hexagons show that their average thicknesses are less than 50 nm and have an RMS roughness of 1.1nm except at the corners

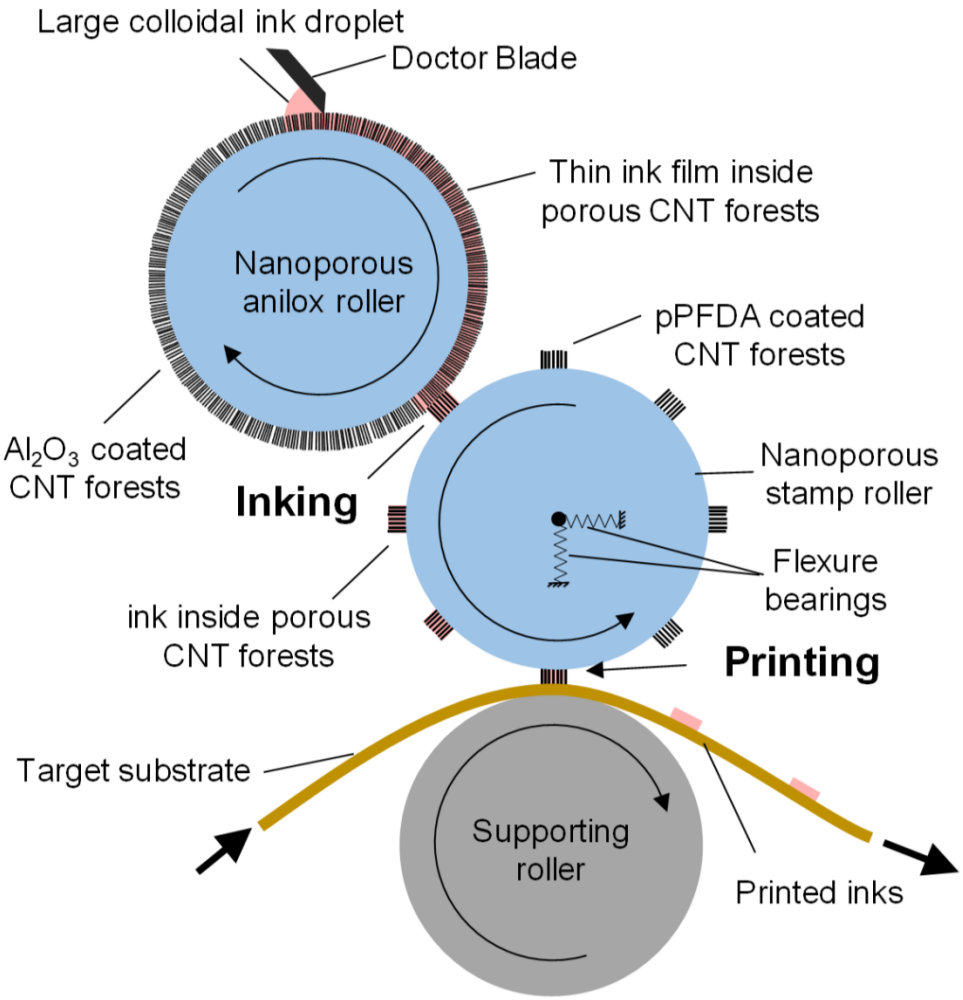

Figure 11: Schematic (not to scale) of proposed laboratory scale continuous roll-to-roll printing system, including the nanoporous stamp roller, a nanoporous anilox roller and a supporting roller.

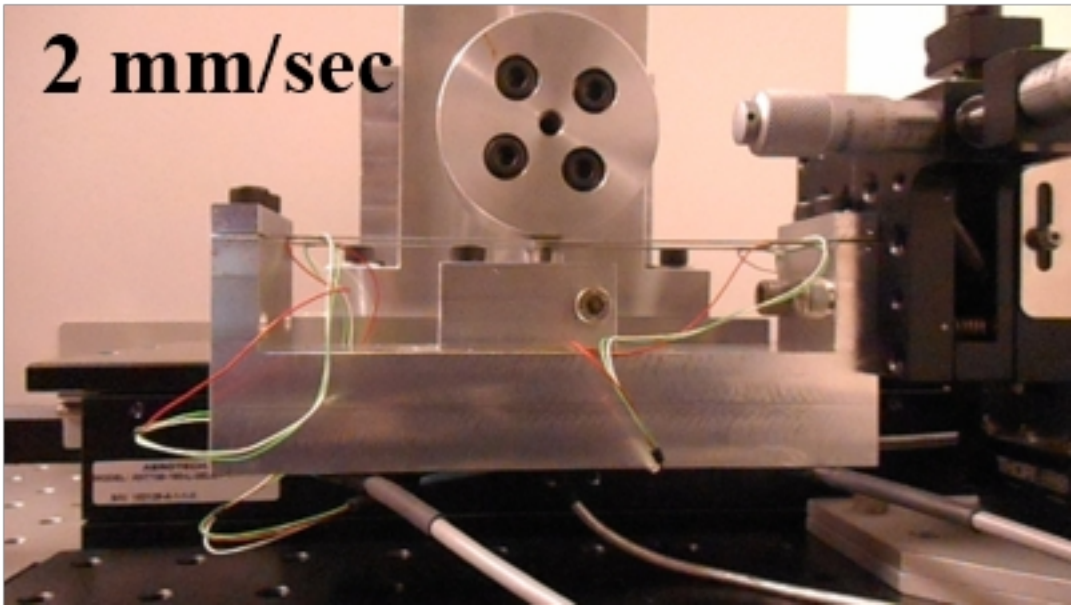
2 mm/sec

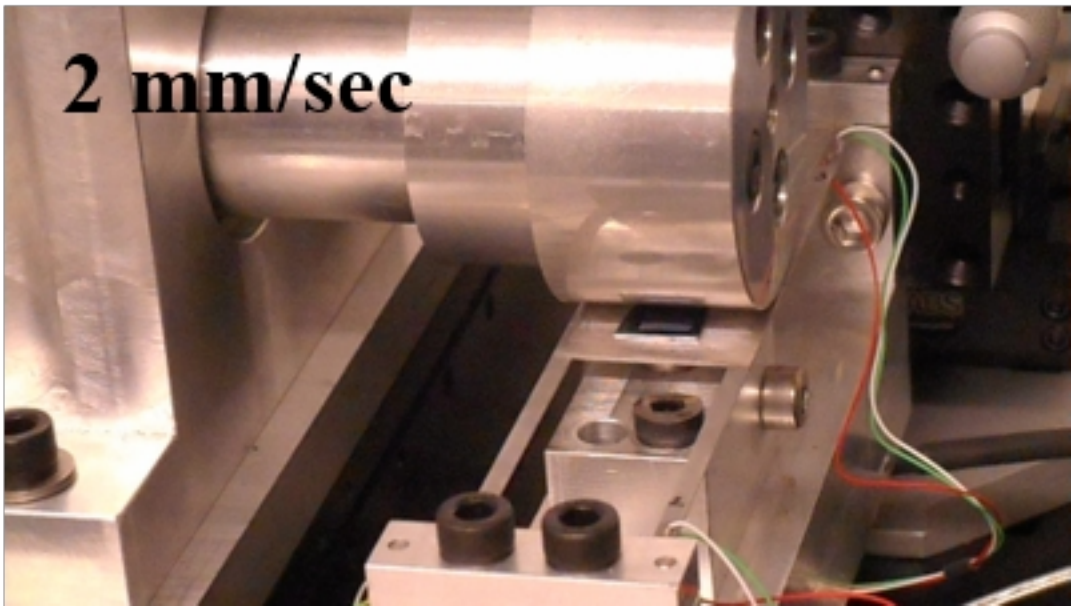
2 mm/sec

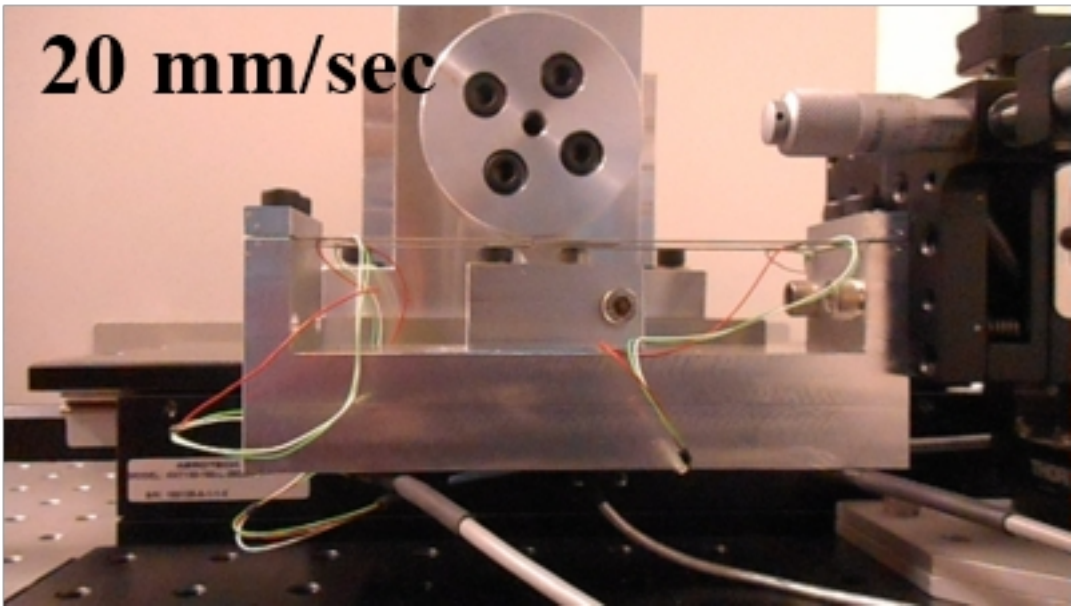
20 mm/sec

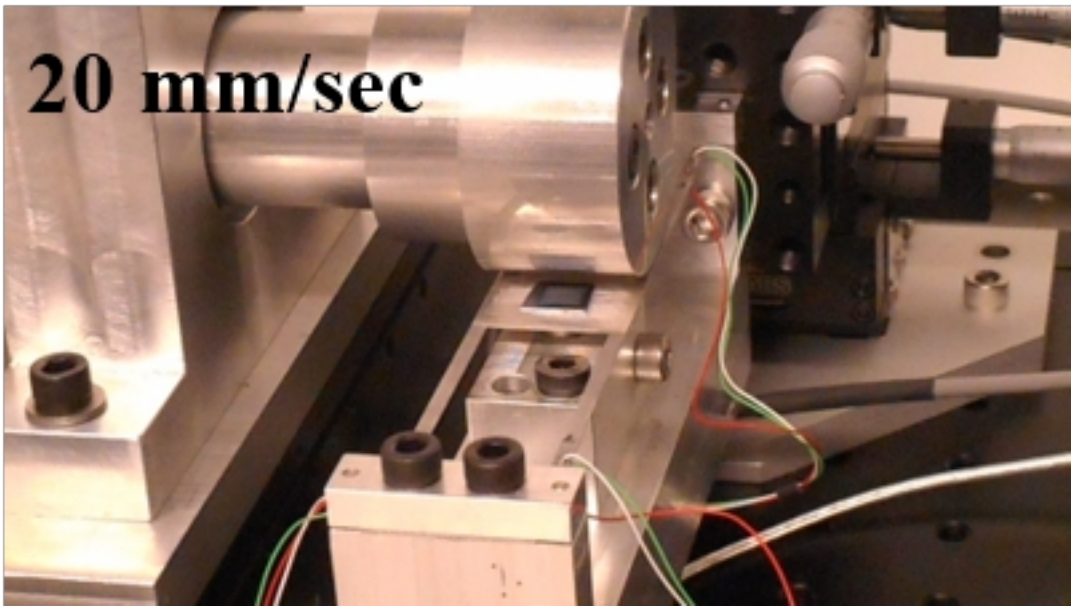
20 mm/sec

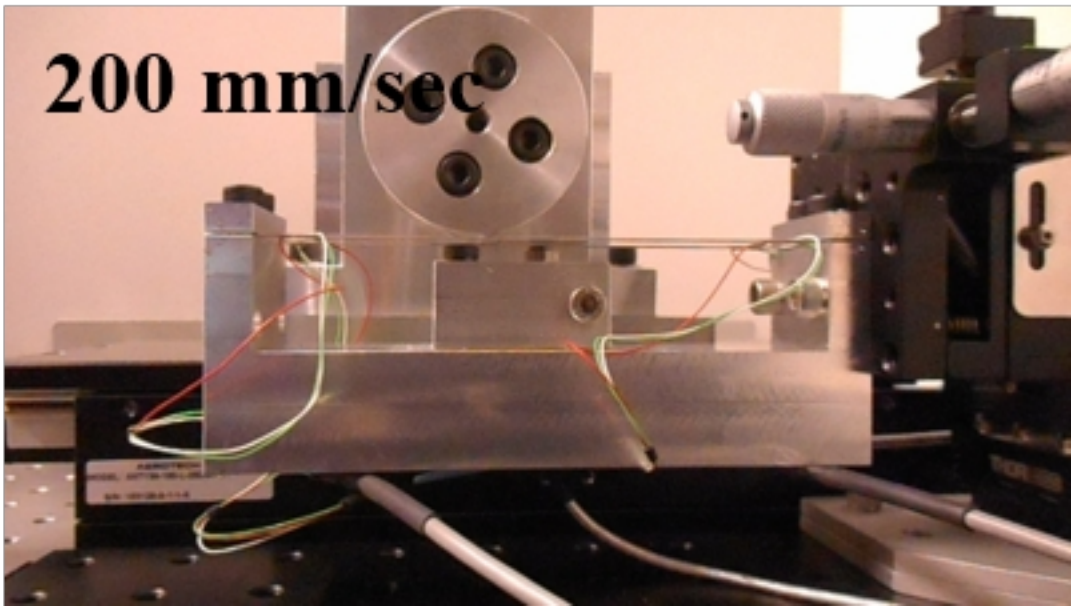
200 mm/sec

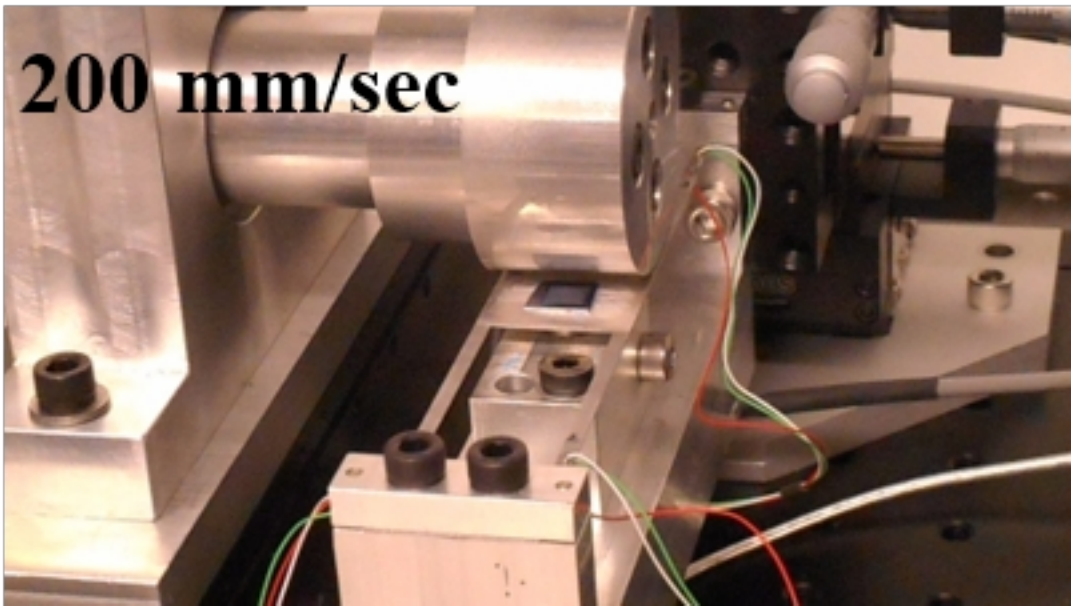
200 mm/sec

Declaration of interests

 The authors declare that they have no known competing financial interests or personal relationships that could have appeared to influence the work reported in this paper.

☐The authors declare the following financial interests/personal relationships which may be considered as potential competing interests:

SUPPORTING INFORMATION FOR

A precision desktop plate-to-roll apparatus for development of advanced flexographic printing processes

Dhanushkodi Mariappan[1], Sanha Kim[1,2], and A. John Hart[1]*

[1]Department of Mechanical Engineering, Massachusetts Institute of Technology, Cambridge, MA 02139, USA.

[2]Department of Mechanical Engineering, Korea Advanced Institute of Science and Technology, Daejeon 34141, South Korea.

*Corresponding author: ajhart@mit.edu

1) Videos

S1A, S1B

The videos S1A and S1B show the front view and side view of the P2R machine printing at 2mm/sec

S2A, S2B

The videos S2A and S2B show the front view and side view of the P2R machine printing at 20mm/sec

S3A, S3B

The videos S3A and S3B show the front view and side view of the P2R machine printing at 200mm/sec

2) First resonant frequency of the flexure

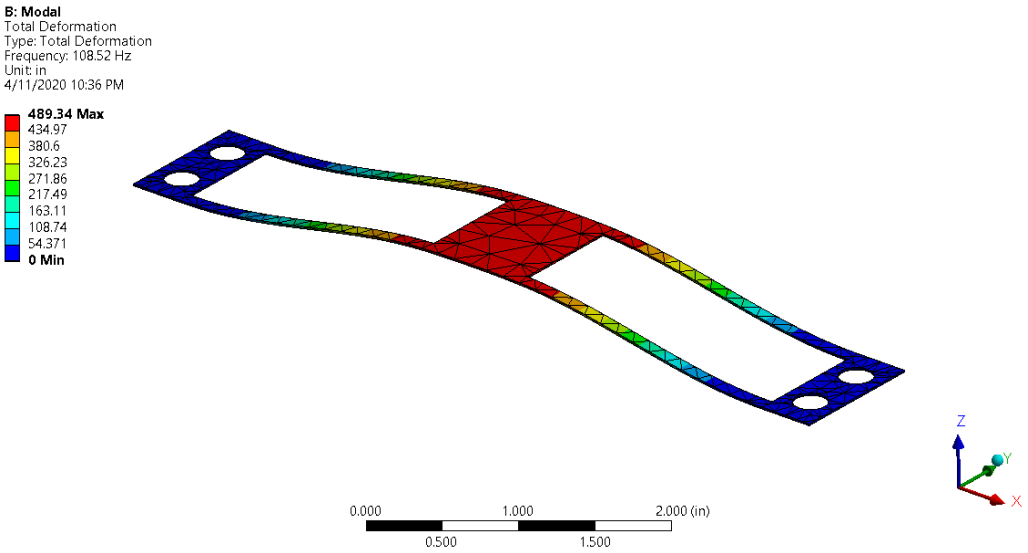

Figure S1. The deflection corresponding to the first mode of the flexure at 108.52 Hz

3) Motor Specifications

Motor	Parameter	Value	Unit
ANT 130 L	Maximum Speed	6.00E+07	counts/sec
	Number of counts	6.40E+06	counts/cycle
	Distance	32	mm/cycle
	Machine resolution	5.00E-06	mm
BMS 60	Maximum Speed	7639438	counts/sec
	Number of counts	4.00E+06	counts/rev
	Distance	157.08	mm/rev
	Machine resolution	3.927E-05	mm

Table S1. Specifications of the linear (ANT 130L) and rotary (BMS 60) motors

4) Error Budget for Printing Force

Error in printing force from flexure deflection due to misalignments and shaft runout is given by

$$K(L\ tan\theta_p + L\ tan\theta_y + \Delta + \Delta_F)$$

where θ_p , θ_y are the pitch and yaw misalignments, Δ is the shaft runout, and Δ_F is the flatness error

The resolution of the pitch-yaw stage is 109.1 arc-seconds.

$\theta_p = \theta_y = \frac{109.1^0}{3600}$; $L = 20\ mm$

Runout, Δ = 5 µm

Flatness error, Δ_F= 1 µm

Error in printing force $\approx$ 6.6 mN

5) Method of calculation of distances using the microscope images

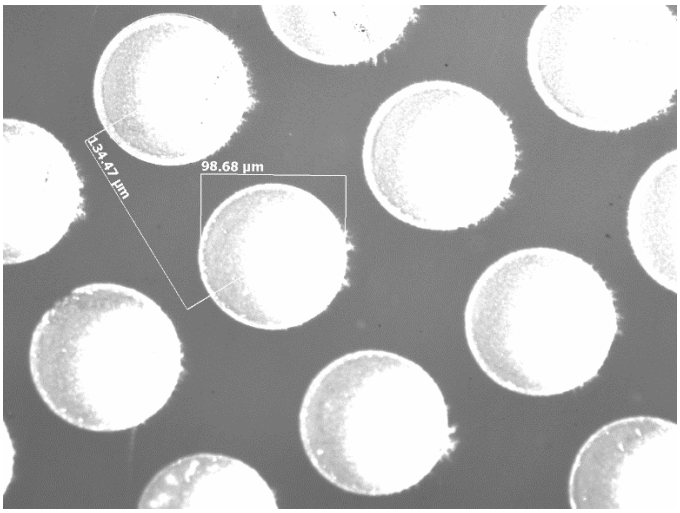

Figure S2. Optical microscope image of printed pattern with distances

Steps

1. The reference dimensions for center to center distance (134.47 µm) and diameter (98.68 µm) were calculated the Zeiss AxioVision software in the Axio Imager Z1 microscope.
2. The areas of the circles (in pixels^2) were calculated using image J.
3. The (x,y) coordinates of the centers of the circles (in pixels) were calculated using image J.
4. The scaling of pixels to distance units (µm) was done using the center to center distance and verified using the diameter measurement (reference dimensions listed in step 1)
5. An example calculation for two circles and their center to center distance is shown below

   Example: To calculate the diameter of a circle and its distance from the reference circle

   Area in pixels for the reference circle, A = 72572 pixels^2

   1 pixel $= \sqrt{\frac{\pi d^2}{4A}} \mu m = 0.3\ \mu m$

Area (pixels)	Diameter (pixels)	Diameter (μm)	X (pixels)	Y (pixels)	Center-center distance (pixels)	Center-center distance (μm)
76708	312.5	101.5	897	311	401.1	130.2
72572	304.0	98.7	555	520	403.1	130.9

Table S2. Calculated center-center distance and diameter from the microscope image

6) Thickness comparison along the sides of the honeycomb patterns

Figure S3 shows the surface profile of the printed honeycomb pattern measured using a laser scanning confocal microscope. On each side of the hexagon, three lines were chosen

along which the profile was measured. For example, on side 1, profile was measured along lines 1A, 1B and 1C. Figure S4 shows the measured profiles along three lines on each of the six sides of the hexagons.

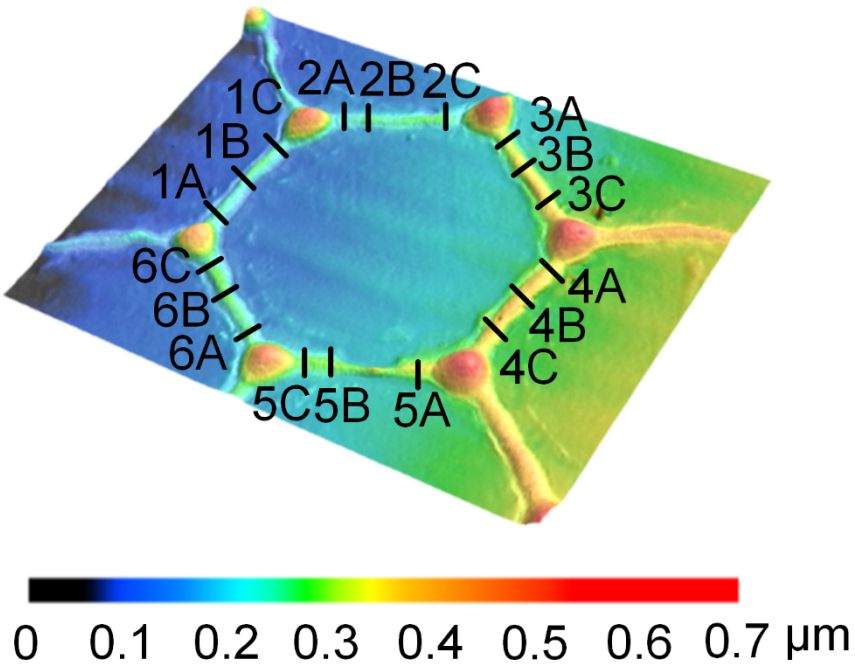

Figure S3. Lines along which the thickness was measured on each of the six sides of the hexagons.

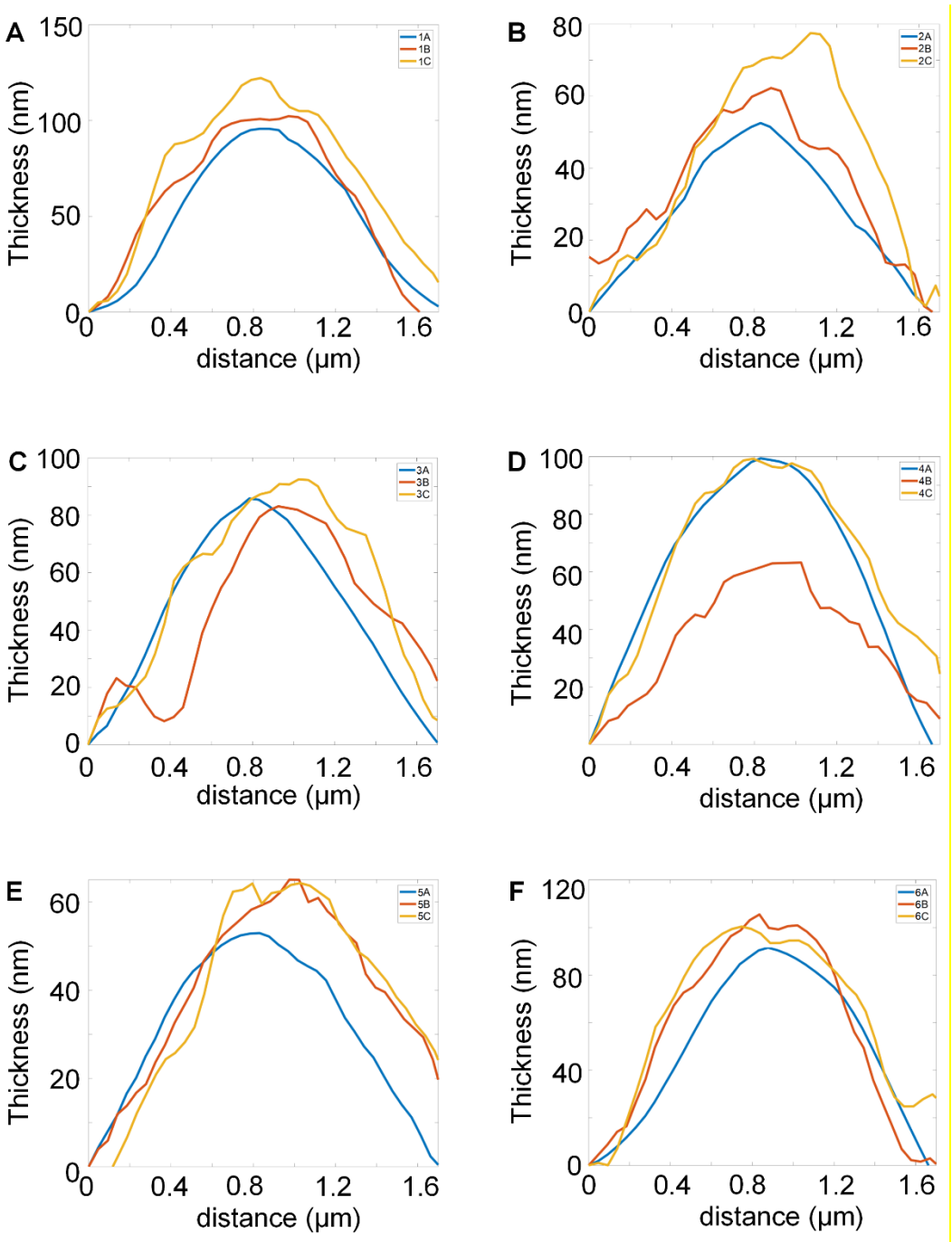

Figure S4. Measured profile of the sides of the hexagons at the three locations A,B,C on A) side 1 B) side 2 C) side 3 D) side 4 E) side 5 F) side 6

	Line 1	Line 2	Line 3	Line 4	Line 5	Line 6
A	56.9	30	40.1	32.5	35.3	52.8
B	47.1	27.5	46.2	60.5	31.1	50.1
C	64.7	37.1	51.5	58	34.7	54.8
Mean	56.2	31.5	45.9	50.3	33.7	52.6
Std. Dev.	7.2	4.1	4.7	12.7	1.9	1.9

Table S3. Calculated average thickness, means and standard deviations from the measured profiles

7) Performance Comparison with other R2R and P2R machines

Reference	Type	Printing method	Print width (cm)	Minimum feature size (µm)	Maximum printing speed (m/min)	Printing force range (N)
This work	P2R	Nanoporous flexography	2	3	12	0.002-0.25
Zhou et al [38]	R2R	Microcontact printing	10.2	0.3	15.2	0-25
Choi et al [39]	R2R	Gravure	Not given	Not given	24	100-1000
Petrzelka et al [40]	P2R	Microcontact printing	10.2	5	1.2	3

Table S4. Comparison of Specifications of the P2R machine with other R2R and P2R printing machines reported in literature